Article

Rheology of Variable Viscosity-Based Mixed Convective Inclined Magnetized Cross Nanofluid with Varying Thermal Conductivity

Adil Darvesh [1], Tanveer Sajid [2], Wasim Jamshed [2], Assad Ayub [1], Syed Zahir Hussain Shah [1], Mohamed R. Eid [3,4,*], Syed M. Hussain [5], Mohammad Akram [5], Muhammad Bilal Hafeez [6] and Marek Krawczuk [6]

[1] Department of Mathematics & Statistics, Hazara University, Manshera 21120, Pakistan
[2] Department of Mathematics, Capital University of Science and Technology (CUST), Islamabad 44000, Pakistan
[3] Department of Mathematics, Faculty of Science, New Valley University, Al-Kharga 72511, Al-Wadi Al-Gadid, Egypt
[4] Department of Mathematics, Faculty of Science, Northern Border University, Arar 1321, Saudi Arabia
[5] Department of Mathematics, Faculty of Science, Islamic University of Madinah, Madinah 42351, Saudi Arabia
[6] Gdańsk University of Technology, Faculty of Mechanical Engineering and Ship Technology, Institute of Mechanics and Machine Design; Narutowicza 11/12, 80-233, Gdańsk, Poland
[*] Correspondence: m_r_eid@yahoo.com

Abstract: Cross nanofluid possesses an extraordinary quality among the various fluidic models to explore the key characteristics of flowing fluid during very low and very high shear rates and its viscosity models depend upon shear rate. The current study establishes the numerical treatment regarding variable viscosity-based mixed convective inclined magnetized Cross nanofluid with varying thermal conductivities over the moving permeable surface. Along with variable thermal conductivities, we considered thermal radiation, thermophoresis, and the Brownian motion effect. An inclined magnetic field was launched for velocity scrutiny and the heat transfer fact was numerically seen by mixed convective conditions. Similarity variables were actioned on generated PDEs of the physical model and conversion was performed into ODEs. Numerical results showed that the frictional force and Nusselt quantity considerably influence the skinning heat transfer processes over the geometry of a moving permeable surface. Furthermore, less velocity was noticed for the greater suction parameter and the Brownian motion parameter corresponds to lower mass transport.

Keywords: variable viscosity; inclined magnetized process; mixed convective cross nanofluid; variable thermal conductivity

1. Introduction

Non-Newtonian fluids have a vital significance in industry, engineering, and daily life, such as in fluid friction reduction, scale-up, and flow tracers, custard, paint, blood, shampoo, molten polymers, starch suspensions, surfactant applications to large-scale heating and cooling systems, melted butter, toothpaste, corn starch, salt solutions, oil–pipeline friction reduction, lubrication and in biomedical flows. Several models [1–8] are established for checking the behavior of non-Newtonian fluids but the most attractive model, Cross fluid, has astonishing key features for investigating the fluid behavior during very high and very low shear rates. No other model can possess such ability in such a situation; due to this factor Cross nanofluid has been recognized as the most important numerical model by recent researchers [9–15]. Azam et al. [16] conducted research on numerical modeling for the changeable thermal characteristics and heat source (sink) in a

Cross nanofluid flowing across a movable cylinder. In this analysis, it was concluded that thermal conductivity makes for higher temperatures. Furthermore, Azam et al. [17] investigated the role of activation energy in the formation of cross-links in the axially symmetric flow of a thermal radiation Cross nanofluid. The importance of bioconvection flow in the Cross nanofluid with multiple slips over the associated wedge geometry is revealed by [18]. In this study, authors utilized gyrotactic motile microorganisms. Haq et al. [19] made their investigation about bio-convection in a Cross nanofluid. in this study, the authors engaged the facts of activation energy, magnetic field, and gyrotactic microorganisms. Magneto Cross fluid associated with bio-convection, activation energy, and gyrotactic microorganisms has been studied [20]. The latest study [21] related to the saturated flow of Cross nanofluid with multiple solutions is made over the vertical thin needle point geometry. Unsteady fluid flow over the Falkner–Skan wedge with its activation energy, nonlinear thermal radiation, and melting heat process is revealed by Waqas et al. [22].

Nanofluid not only makes heat transmission possible but also reduces energy consumption. Because of its importance in biological molecules, scientists are working in several ways to improve it, such as in heat management or energy storage systems, nano cryotherapy, electric generation, heat transfer, and so on. The first-time revelation of the nanofluids concept was established by Choi et al. [23] and for the first time it is established that nanofluid-containing nanoparticles can enhance thermal conductivity. Said et al. [24] published their article on the issue of recent advances in nanofluids with exergy, solar energy, environmental impact, and economic analysis. Sheikholeslami et al. [25] did work on the progress on photovoltaic systems and flat plate solar collectors in nanofluid. A numerical study related to the magneto-convective flow considered nanoparticles of copper–water nanofluid and entropy generation with Chamfers, by Marzougui et al. [26]. The significance of nonlinear thermal radiation and activation energy in a 3D mathematical model of Eyring–Powell nanofluid is presented by Muhammad et al. [27]. Studies related to fundamental and physical stability, heat transport, thermophysical properties, dynamic motion, and applications, as well as the challenges of nanofluids, are described by Said et al. [28]. Meibodi et al. [29] analyzed the second law analysis of a nanofluid-based solar collector using experimental data. Furthermore, many other scholars [30,31] performed investigations related to the financial and environmentally friendly analysis of metallic oxide nanoliquid and the applications of nanofluids in solar energy.

There are many research articles on Cross fluid associated with several effects, but variable viscosity and variable thermal conductivity with the inclined magnetized flow are still not investigated as they should be so, the current study established the numerical treatment regarding variable viscosity based on a mixed convective inclined magnetized Cross nanofluid with varying thermal conductivity over the moving permeable surface. Along with variable thermal conductivity, we considered thermal radiation, thermophoresis, and the Brownian motion effect. An inclined magnetic field was launched for velocity scrutiny and the heat transfer fact was numerically observed by mixed convective conditions.

2. Viscosity Model of Cross Nanofluid

The Cauchy stress tensor for the case of a four-parameter fluid can be defined as

$$\tau = -pI + \mu(\dot{\gamma})A_1 \tag{1}$$

The shear rate term comprising of zero and infinite shear rate viscosities along with shear power-law index n and material time constant Γ is given by

$$\mu(\dot{\gamma}) = \left[\mu_\infty + (\mu_o - \mu_\infty)[1 + (\Gamma\dot{\gamma})^n]\right]. \tag{2}$$

The first Rivilin–Ericksen tensor is given by

$$\left(\dot{\gamma} = \sqrt{\frac{1}{2} tr(A_1)^2}, A_1 = (\nabla V) + (\nabla V)^T\right) \tag{3}$$

3. Orientation and Formulation of Physical Problem

It is considered that the 2D Cross nanofluid is flowing, facing a stagnation point in a porous medium. Furthermore, fluid is considered to be incompressible very near to the stagnation point and the surface coincides with the plane of equation $y = 0$. The zero-mass flux and mixed convective temperature conditions can be considered at the boundary surface of the sheet. The active and passive controls of nanoparticles at the surface of the sheet are controlled by zero mass flux nanoparticle conditions. The stagnation point is at the point O. The fluid region is taken as $y > 0$, and the above sheet is porous, which can be seen in Figure 1. Continuity, momentum, temperature, and concentration equations are derived from the law of conservation of momentum, Navier Stoke's equation, the second law of thermodynamics, and Fick's second law of diffusion respectively. The variation in fluid, temperature and concentration are monitored with the utilization of variable viscosity [32], variable thermal conductivity [33,34], and variable molecular diffusivity phenomena, respectively. The governing system of equations in the light of the above-mentioned assumptions is given below.

$$u_x + v_y = 0 \tag{4}$$

$$\rho_f[uu_x + vv_x] = \frac{\partial}{\partial y}\left\{\frac{\mu_0}{[1 + \Gamma^2(u_y)]^n}\right\} + \frac{\sigma B_0^2}{\rho}\sin^2(\omega)\,(u - u_e) + u_e\frac{du_e}{dx} + g\beta_T(T - T_\infty) \tag{5}$$

$$[uT_x + vT_y] = \frac{1}{\rho c_p}\frac{\partial}{\partial y}\left[K(T)T_y\right] + \tau\left[D_B T_y C_y + \frac{D_T}{T_\infty}\left[(T_y)^2\right]\right] + \frac{16\sigma^*}{3k^*\rho c_p}\left[\frac{\partial}{\partial y}(T_y T^3)\right] \tag{6}$$

$$[uC_x + vC_y] = \frac{1}{\rho c_p}\frac{\partial}{\partial y}\left[D(C)C_y\right] + \left[D_B C_{yy} + \frac{D_T}{T_\infty}(T_{yy})\right] \tag{7}$$

where $\begin{bmatrix} K(T) = k_\infty\left\{1 + \varepsilon_1\frac{(T - T_\infty)}{\Delta T}\right\}, and\ D(C) = D_\infty\left\{1 + \varepsilon_2\frac{(C - C_\infty)}{\Delta C}\right\} \\ \frac{1}{\mu} = \frac{1}{\mu_\infty}[1 + \gamma_1(T - T_\infty)], or\ \frac{1}{\mu} = \alpha\{T - T_\Gamma\} \end{bmatrix}$.

Following the boundary conditions must be considered for Equations (4)–(7).

$$\left.\begin{aligned} & u_w = cx, -K(T)T_y = (T - T_W), v = v_w, \left[D_B C_y + \frac{D_T}{T_\infty}(T_y)\right] = 0, at\ y = 0, \\ & C \to C_\infty, u \to u_e = ax, T \to T_\infty, as\ y \to \infty \end{aligned}\right\} \tag{8}$$

The system of PDE (4)–(8) is passed through these similar transformations

$$\left.\begin{aligned} & u = xcf'(\eta), \quad \eta = y\left(\frac{\upsilon}{c}\right)^{-1/2}, v = -\sqrt{c\upsilon}f(\eta) \\ & \theta(\eta) = \frac{T - T_\infty}{T_w - T_0}, \phi(\eta) = \frac{C - C_\infty}{C_w - C_0} \end{aligned}\right\} \tag{9}$$

$$f'''(1 + (we_1 f'')^n)^{-2}\{[1 - (n-1)(Wef'')^n]\} + f''\left(\frac{\theta'}{\theta_r - \theta}\right) - \left(\frac{\theta_r - \theta}{\theta_r}\right)[f'^2 - ff'' + G\theta + A^2 - 1 - M^2\sin^2(\omega)f']$$
$$= 0 \tag{10}$$

$$(1 + \varepsilon_1)\theta'' + \varepsilon_1\theta'^2 + \frac{4}{3}N\frac{d}{d\eta}\left[\{\theta(\theta_f - 1) + 1\}^3\theta'\right] + Pr[Nb\phi'\theta' + N_t\theta'^2 + (f\theta' - f'\theta)] = 0 \tag{11}$$

$$(1 + \varepsilon_2)\phi'' + \varepsilon_2\phi' + \frac{N_t}{N_b}\theta'' + Sc(f\phi' - f'\phi) = 0 \tag{12}$$

$$\left.\begin{aligned} & f = s, f' = 1, \theta' = -\gamma(1 - \theta), N_b\phi' + N_t\theta' = 0\ at\ \eta = 0 \\ & f' \to A, \theta \to 0, \phi' \to 0, as\ \eta \to \infty \end{aligned}\right] \tag{13}$$

After the reduction of PDEs into ODEs, there are some physical parameters that appear in the system of ODEs.

$$
\left.
\begin{aligned}
&We = (\Gamma^2 x^2 c^3)/v, s = v_w/\sqrt{cv}, Pr = v/\alpha, \\
&\theta_r = (T_r - T_\infty)/(T - T_w) = (-1)/\gamma(T - T_\infty), \\
&G = Gr_x/(Re_x^2) = (g\beta_T b)/c^2, M = \frac{\sigma B_0^2}{\rho a} \\
&N_t = (\tau D_T(T_w - T_\infty))/(vT_\infty), N_b = (\tau D_T(C_w - C_\infty))/v, \\
&A = a/c, Gr_x = (g\beta_T(T_w - T_\infty)x^3)/v^2, \\
&Re_x = \frac{u_w(x)}{v}, N = \frac{4\sigma^* T_\infty^3}{k^* k_\infty}
\end{aligned}
\right\}
\tag{14}
$$

$$D_B \frac{\partial C}{\partial y} + \frac{D_T}{T_\infty}\frac{\partial T}{\partial y} = 0 \qquad\qquad -K(T) = \frac{\partial T}{\partial y}(T - T_w)$$

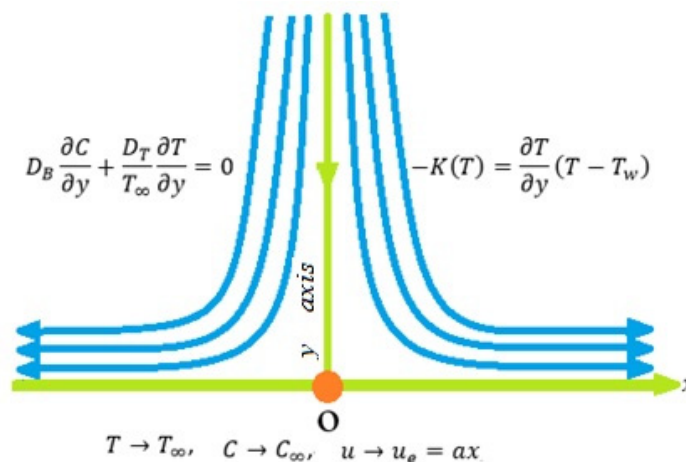$$T \to T_\infty, \quad C \to C_\infty, \quad u \to u_e = ax$$

Figure 1. Flow scheme.

4. Methodology

The above-obtained ODEs can be handled numerically with the assistance of the Lobatto IIIA MATLAB built-in scheme. In this scheme, the nonlinear model is converted into ODEs with the help of suitable transformations. The dimensionless ODEs are reduced into the first order by taking suitable variables and solving these first-order ODEs with the help of the Lobatto IIIA scheme. The detailed flow chart of the Lobatto IIIA scheme is given below. In the first step the nonlinear PDEs comprise distinguished effects such as the stagnation point, varying viscosity, temperature, changing conductivity, the Buongiorno model comprising nanoparticles, nonlinear based warmth radiation, variation in molecular diffusivity, zero mass flux, and temperature convection. These modeled PDEs are renovated into dimensionless ODEs by considering suitable self-transformations. The dimensionless PDEs are transformed into first-order ODEs by adopting suitable variables as shown in the equations below. These first-order ODEs are handled numerically with the utilization of the Lobatto IIIA MATLAB built-in scheme. The graphical analysis in terms of figures and tables was carried out in the case of various dimensionless parameters that appeared during the numerical simulation of the problem against velocity, temperature, concentration, skin friction coefficient, and Nusselt numbers. The conversion of modeled PDEs regarding mass, momentum, temperature, and concentration into dimensionless ODEs was performed by the procedure mentioned below.

$$f = w_1, \tag{15}$$

$$f' = w_2, \tag{16}$$

$$f'' = w_3, \tag{17}$$

$$f''' = \left(\frac{\theta_r - w_4}{\theta_r}\right)(w_2{}^2 - w_1 w_3 + G w_4 + A^2 + 1 M^2 \sin^2(\omega)\, w_2) + w_3 \left(\frac{w_5}{\theta_r - w_4}\right)$$
$$+ (1 + (We w_3)^n)^{-2}(1 - (n-1)(We w_3)^n) \tag{18}$$

$$\theta' = w_5, \tag{19}$$

$$\theta'' = \frac{-(\varepsilon_1 w_5{}^2 + \Pr(w_1 w_5 + w_2 w_4) + \Pr(N_b w_5 w_7 + N_t w_5{}^2))}{\left((1 + \varepsilon_1) + \frac{4}{3} N(1 + (\theta_f - 1)w_4)^3\right)}, \tag{20}$$

$$\phi' = w_7, \tag{21}$$

$$\phi'' = \frac{Sc\,(w_2 w_7 - Sc\, w_1 w_6) - \left(\frac{Nt}{Nb}\right) w_6{}' - \varepsilon_2 w_7}{1 + \varepsilon_2}, \tag{22}$$

$$\left.\begin{array}{l} \eta = 0 : w_1(\eta) = s, w_2 = 1, w_5(\eta) = -\gamma(1 - w_4), N_b w_7 + N_t w_5 = 0, \\ \eta \to \infty: w_2(\eta) \to A, w_4(\eta) \to 0, w_6(\eta) \to 0. \end{array}\right\} \tag{23}$$

The Lobatto IIIA scheme [35,36] is adopted here to fetch the numerical solution of an assumed problem and its general procedure is explained by a chart in Figure 2.
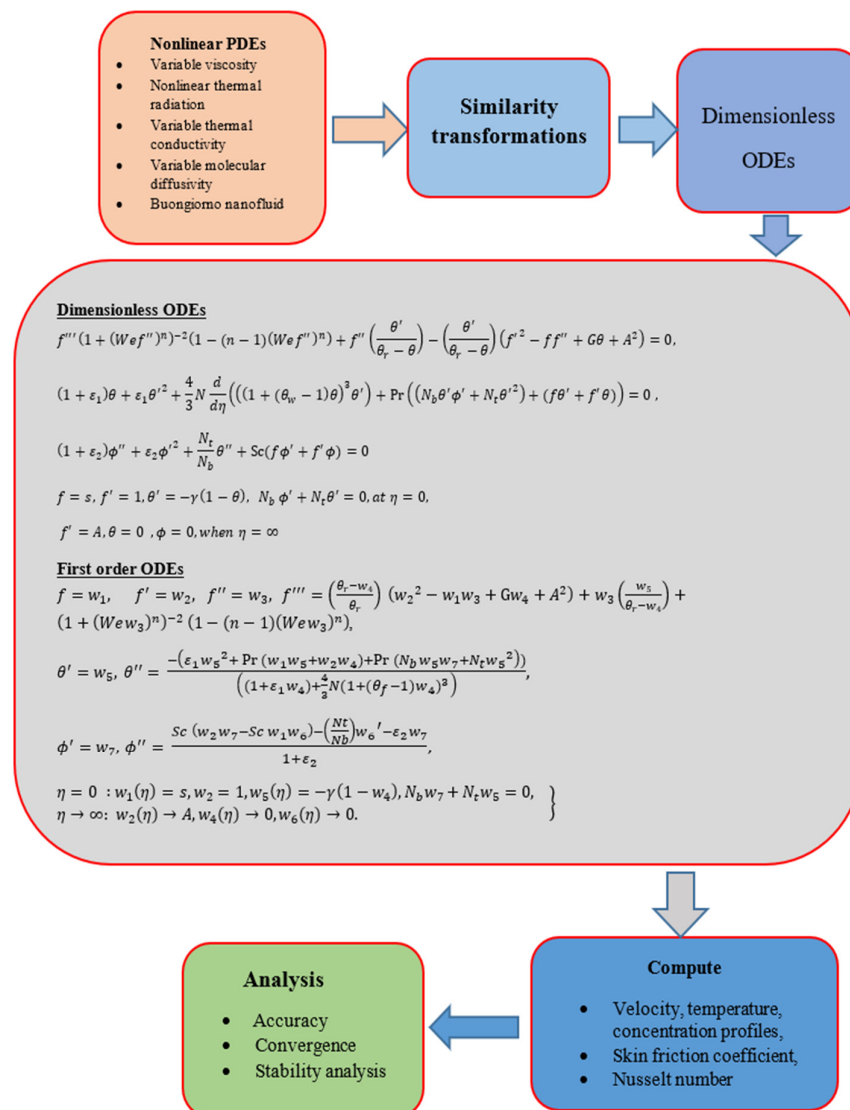

Figure 2. Flow chart of Lobatto IIIA scheme.

5. Comprehensive Debate Based on Numerical Results

This segment has been launched to discuss the impact of several physical factors on the rapidity, temperature, and concentricity outlines. The engineering amounts of attention such as the frictional force and Nusselt quantity were calculated and portrayed in the form of figures and tables.

Figure 3 is constructed to study the effect of unsteadiness parameter A on the rapidity field in the absence (presence) of an inclination angle. It is quite evident that amplification in the unsteadiness parameter brings about an increment change in the fluid velocity. The inclination angle magnifies due to magnification in A, which escalates the fluid flow and the velocity field. The effect of the Grashof number G on the velocity field in the absence (presence) of the inclined angle ω is highlighted in Figure 4. The Grashof number is the ratio of buoyancy forces to the viscous forces. A positive change in G intensifies the buoyancy forces instead of viscous forces. The density of the fluid diminishes owing to an enrichment in G, which lessens the fluid viscosity and magnifies the fluid velocity. The velocity of fluid diminishes by the virtue of magnification in the power-law index n as shown in Figure 5. The parameter n decides how viscous the fluid is. Fluid behavior in the case of $n < 1$ is shear thinning, $n = 1$ is Newtonian, and $n > 1$ is shear thickening. The fluid becomes much dense, and viscosity amplifies due to an increase in n which brings about an abatement in $f'(\eta)$. An incremental change in electrical conductivity allows more current to flow through the fluid which creates a resistive force termed Lorentz force, which depreciate the fluid motion and furthermore diminish $f'(\eta)$ as shown in Figure 6. Figure 7 reveals the influence of the Weissenberg number We on $f'(\eta)$. The parameter We represents the relaxation time, the time in which the fluid deforms to regain its original shape. During that time the viscosity of the fluid increases, which depreciates the fluid velocity. The Weissenberg number is the ratio of elastic forces to viscous forces. The fluid becomes more viscous by escalating We which lessens the fluid motion and $f'(\eta)$. The heat transfer coefficient γ is determined by the transfer of heat from one place to another and the heat transfer rate amplifies on the behalf of magnification in γ as shown in Figure 8. It is observed that the rate of convective heat transfer is proportional to the temperature difference. A positive variation in γ provides substantial heat which is absorbed by the system and amplifies the temperature field. Radiation is one of the modes of heat transfer, with the other two being conduction and convection. Nonlinear thermal radiation is employed where the elevated temperature change is required and has immense utilization in an industry such as polymer fabrication, combusting apparatuses, satellites, etc. Thermal radiation is directly related to the temperature difference. The temperature of the fluid escalates because of a positive change N which enhances the temperature field $\theta(\eta)$ as shown in Figure 9. Figure 10 investigates the impact of the Prandtl number on $\theta(\eta)$. The Prandtl number is a ratio of momentum diffusivity to thermal diffusivity. It is observed that the thermal diffusivity of nanoparticles lessens because of magnification of the Prandtl number Pr, which depreciates the temperature of the fluid and heat transfer rate. From Figure 11 it is observed that the temperature field amplifies owing to amplification in θ_w. The parameter θ_w is an important part of nonlinear thermal radiation along with N. It is observed that the nonlinear thermal radiation term $(1 + (\theta_w - 1)\theta)^3$ escalates by increasing θ_w, which augments the energy equation and temperature field and the overall heat transfer rate of the fluid. Figure 12 displays the effect of Brownian diffusion, N_b, on the concentration field $\phi(\eta)$. Brownian diffusion is one of the important parameters of the Buongiorno nanofluid model. Brownian diffusion is inversely related to the concentration phenomenon. Incremental change in the Brownian motion parameter N_b lessens the concentration phenomenon, which diminishes the concentration field $\phi(\eta)$. Figure 13 is designed to study the impact of thermal conductivity ε_1 on $\phi(\eta)$. In fluids, thermal conductivity takes place due to intermolecular collision. Molecules collide more randomly because of magnification in ε_1. The molecules shift kinetic energy, which amplifies the fluid temperature and diminishes the concentration of the fluid and $\phi(\eta)$. The thermophoresis parameter N_t is inversely related to $\phi(\eta)$. The

concentration boundary layer thickness expands owing to an increment in N_t (Figure 14). The concentration of the fluid decreases when the thermophoretic parameter is increased. The impact of raising the thermophoretic parameter is restricted to increasing the concentration profile wall slope. The Schmidt number Sc plays the same role in mass transfer rate as Pr in the heat transfer rate. The Schmidt number is a ratio of mass diffusivity to mass diffusivity. Diffusivity is related to the concentration and Schmidt Sc is inversely related to the diffusion phenomenon. A positive variation in Sc diminishes the diffusion phenomenon, which lessens the concentration and moreover $\phi(\eta)$ (Figure 15).
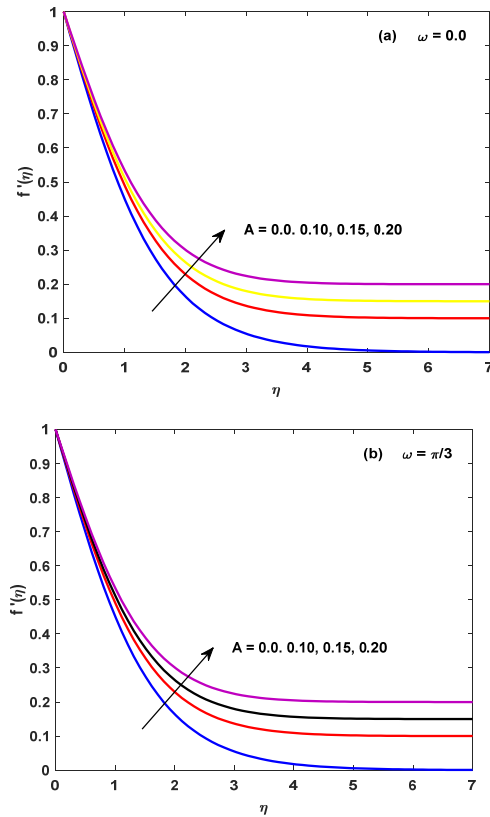
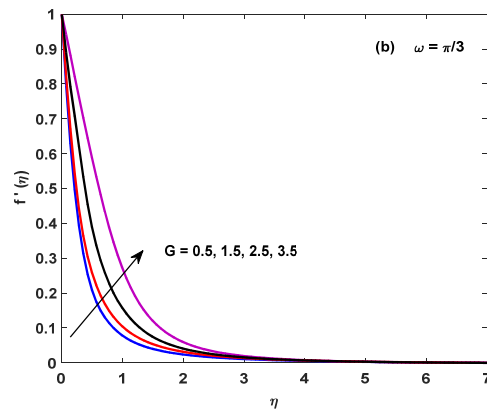**Figure 3.** (**a**,**b**) Linkage of A with velocity distribution at $\omega = 0$ and $\omega = \pi/3$.
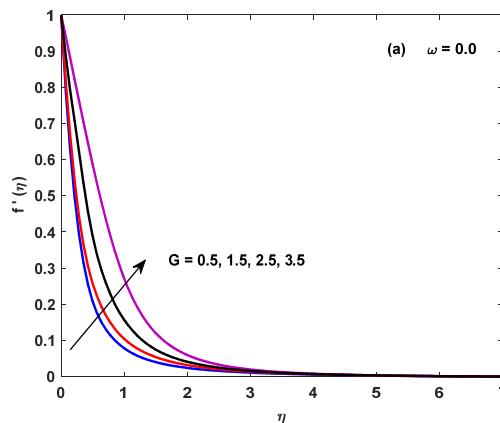
Figure 4. (**a**,**b**) Linkage of G with velocity distribution at $\omega = 0$ and $\omega = \pi/3$.
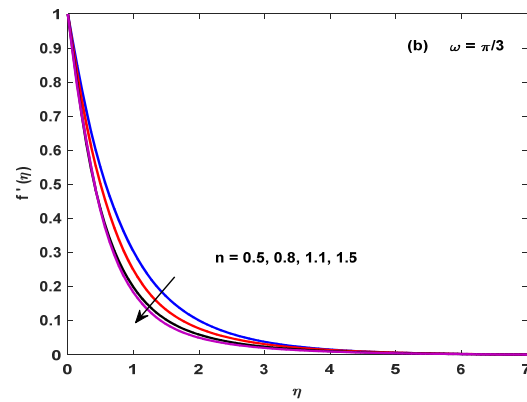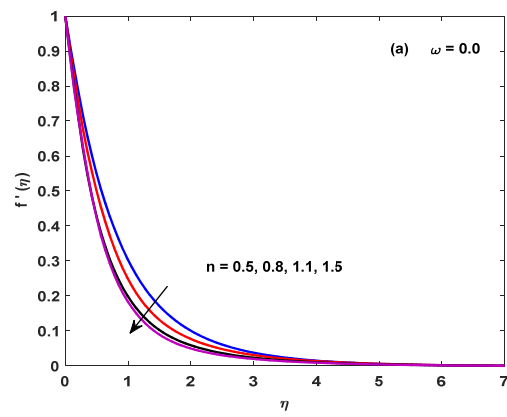

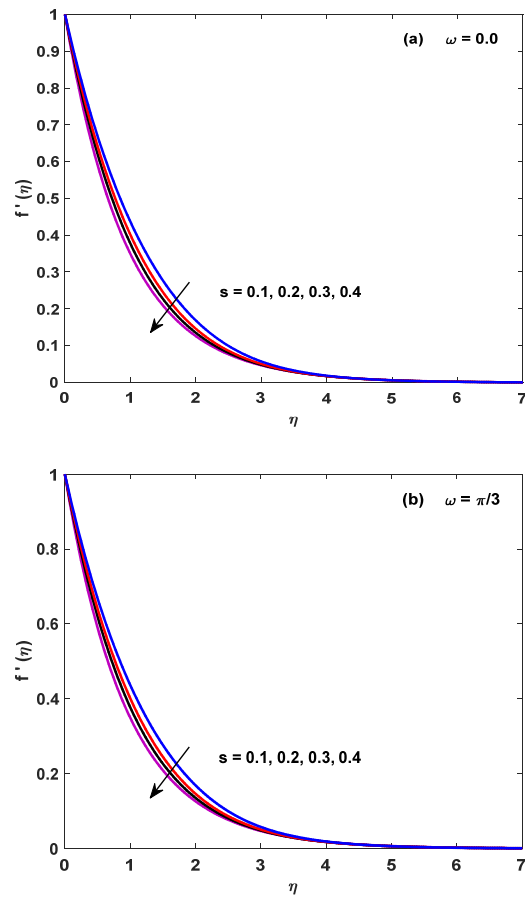**Figure 5.** (**a**,**b**) Linkage of n with velocity distribution at $\omega = 0$ and $\omega = \pi/3$.
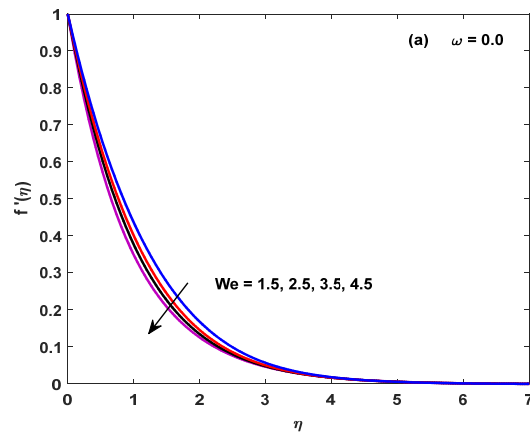
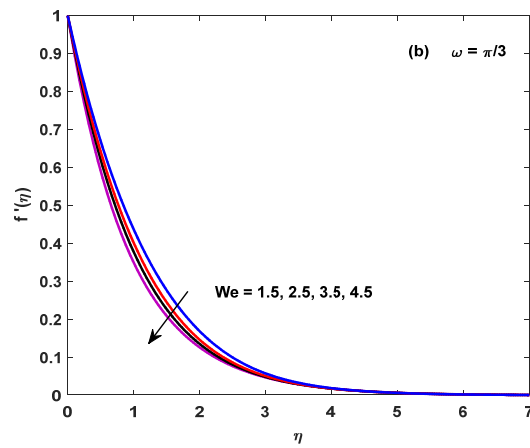**Figure 6.** (**a**,**b**) Linkage of s with velocity distribution at $\omega = 0$ and $\omega = \pi/3$.

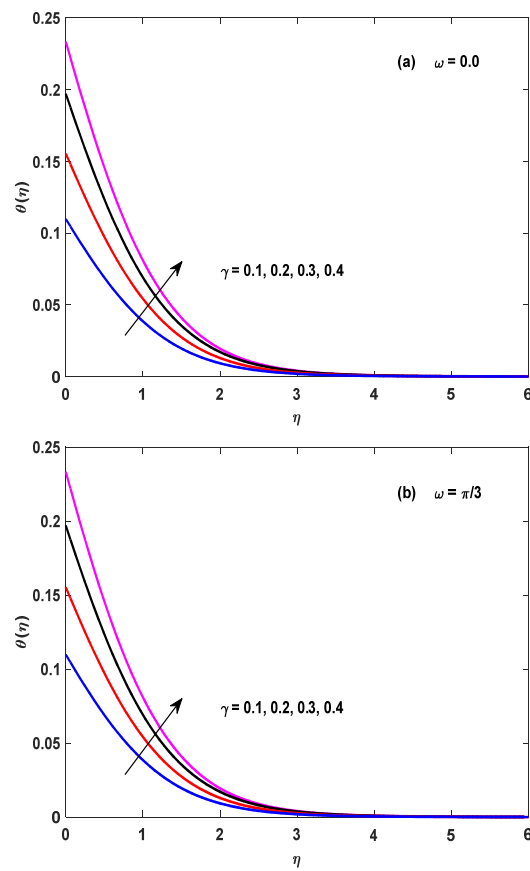**Figure 7.** (**a**,**b**). Linkage of We with velocity distribution at $\omega = 0$ and $\omega = \pi/3$.

Figure 8. (**a**,**b**) Linkage of γ with temperature distribution at $\omega = 0$ and $\omega = \pi/3$.
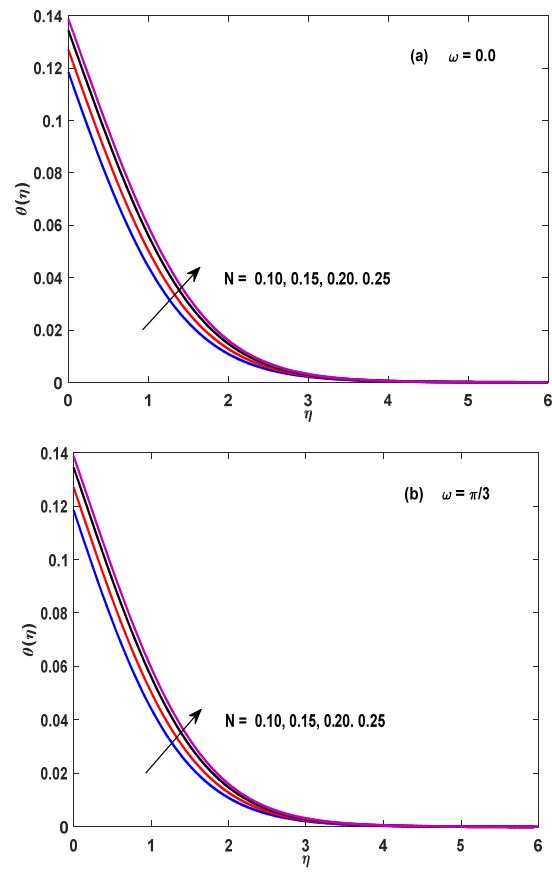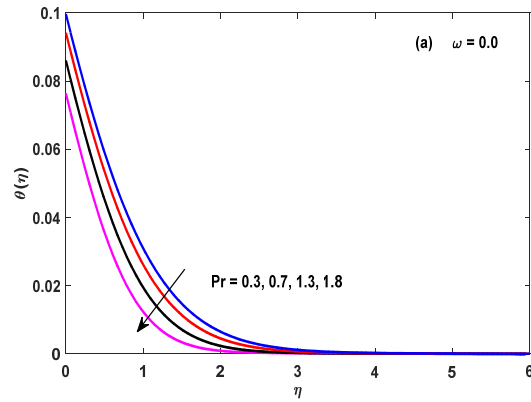
Figure 9. (**a**,**b**) Linkage of N with temperature distribution at $\omega = 0$ and $\omega = \pi/3$.

Figure 10. (**a**,**b**) Linkage of Pr with temperature distribution at $\omega = 0$ and $\omega = \pi/3$.
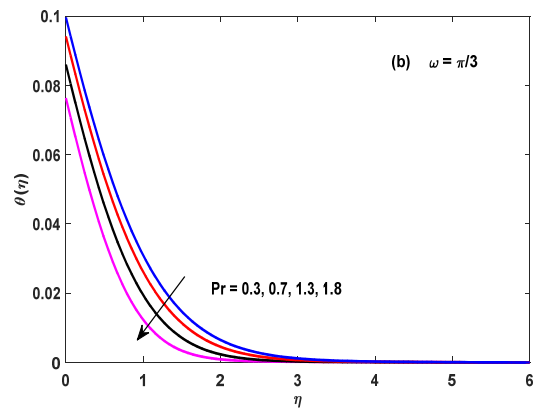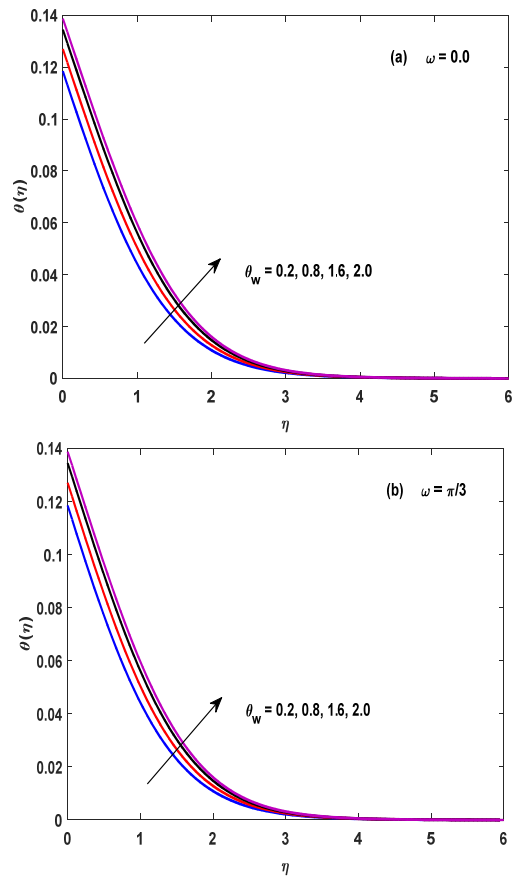

Figure 11. (**a**,**b**) Linkage of θ_w with temperature distribution at $\omega = 0$ and $\omega = \pi/3$.

Figure 12. (**a**,**b**) Linkage of N_b with concentration distribution at $\omega = 0$ and $\omega = \pi/3$.

Figure 13. (**a**,**b**) Linkage of ε_1 with concentration distribution at $\omega = 0$ and $\omega = \pi/3$.

Figure 14. (**a**,**b**) Linkage of N_t with concentration distribution at $\omega = 0$ and $\omega = \pi/3$.
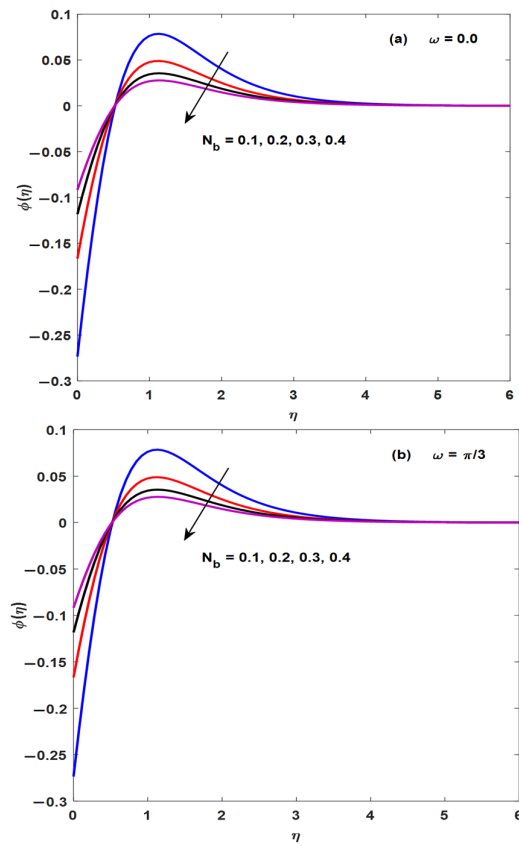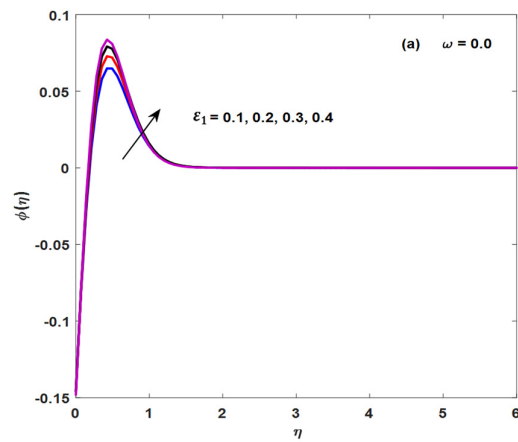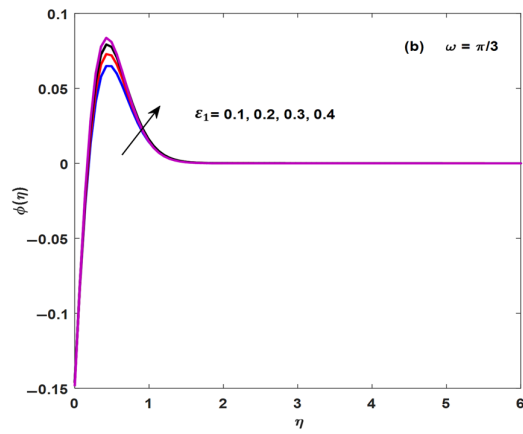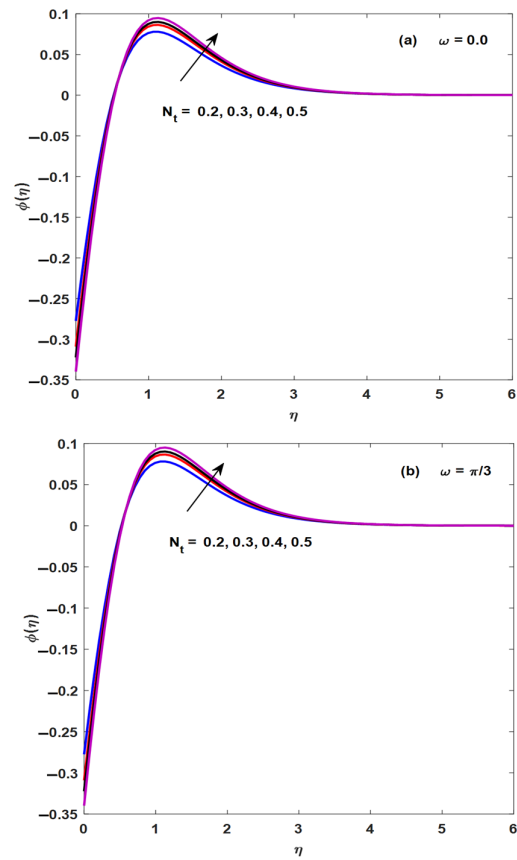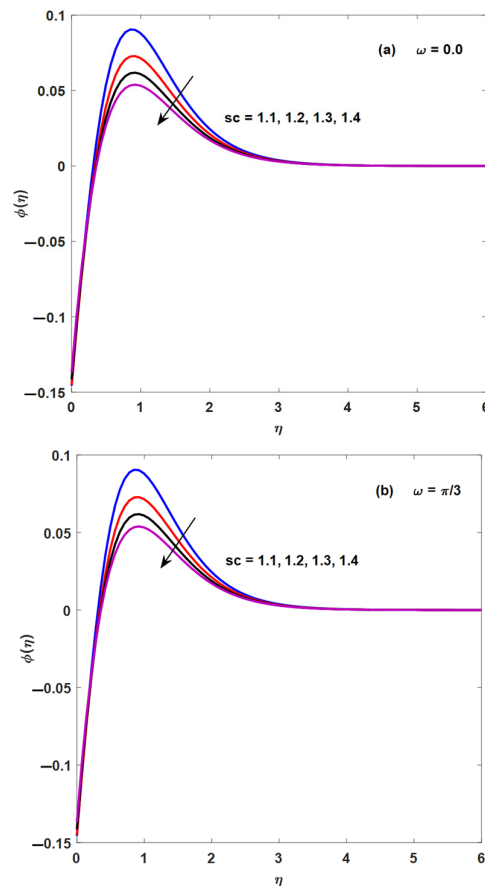
Figure 15. (**a**,**b**). Linkage of *Sc* with concentration distribution at $\omega = 0$ and $\omega = \pi/3$.

6. Validity of This Study

Table 1 is designed to present the comparative analysis of the obtained results with Hayat et al. [37]; an examination which probed the unsteadiness flowing of Powell-Eyring liquid via an angled stretchable plate was investigated in this paper by employing the homotopy analysis technique in the existence of thermal radiation. Additionally, we compared our results with a non-uniformly heat-generating study by Waqas et al. [38], which elaborated on the unsteadiness magnetic hydrodynamical (MHD) stagnating point, flowing via a porousness shrinkable plate of Casson fluid, flowing with radiative fluxing transference by the shooting method. We also compared our results with Raghunath et al. [39], an investigation which discussed the Soret effects on unsteady magnetohydrodynamics flowing across a semi-infinite vertical penetrable moveable plate with thermal radiative, heat absorptive, and homogeneous chemically reactive samples exposed to changing suction by the Runge-Kutta 4th-order computational technique, in limiting cases by taking variation in unsteady parameter A. From the table, it is observed that the obtained computational outcomes for the case of the present model with the utilization of the current numerical technique are in good agreement with the available literature.

Table 1. Validness of the current scheme.

A	Ref. [37]	Ref. [38]	Ref. [39]	Present
0.01	−0.9963	−0.998024	−0.99803	−0.99803
0.02	−0.993	−0.995783	−0.99578	−0.99578
0.05	−0.983	−0.98758	−0.98758	−0.98759
0.1	−0.9603	−0.969386	−0.96938	−0.96938

0.2	−0.908	−0.918107	−0.91811	−0.91811
0.5	−0.6605	−0.66726	−0.66726	−0.66726
1	0.000001	0.000001	0.000001	0.000001
2	2.0181	2.01767	2.01762	2.01761
3	4.72000	4.72964	4.72967	4.72969
Standard Deviation	3.496456	3.496479	3.496489	3.496507

Figure 16 displays the graphical comparison analysis of the obtained results with the already-available literature. The graphical comparison analysis tells us that the obtained results are quite authentic and satisfactory.
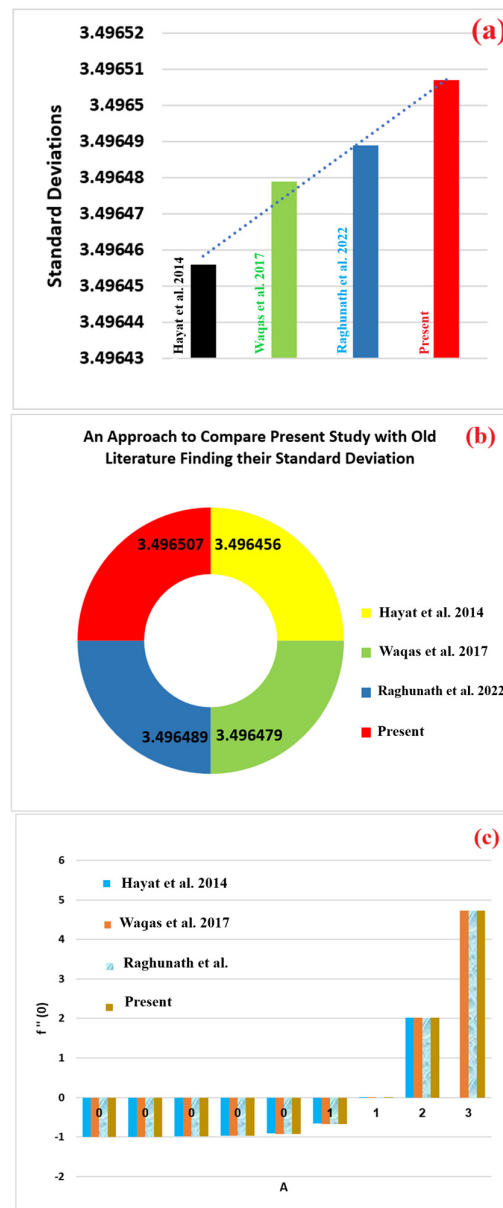
Figure 16. (**a**–**c**) Statistical results of validity with Refs. [37–39].

Figure 17 investigates the effect of We and θ_r on the frictional force coefficient. The surface drag coefficient decreases by increasing We and θ_r. The viscosity of fluid increases by rising We and the fluid becomes more viscous by increasing θ_r. As a result,

the skin friction coefficient diminishes. The effect of Grashof number G and power-law index on the surface drag coefficient is highlighted in Figure 18. The buoyancy forces dominate the viscous fluid by increasing G, which amplifies the skin friction coefficient, and the density of fluid lessens by improving the power-law index, which strengthens the surface drag coefficient phenomenon.
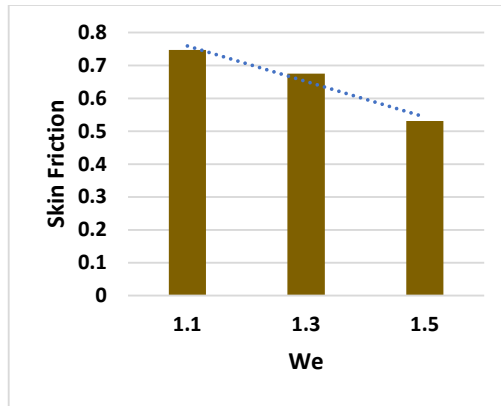
(a)
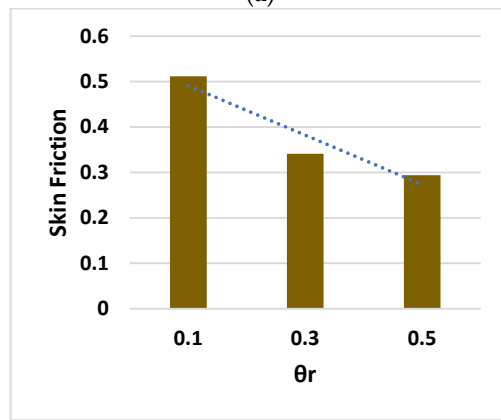
(b)

Figure 17. (**a**,**b**) We and θ_r attachment with skin friction.
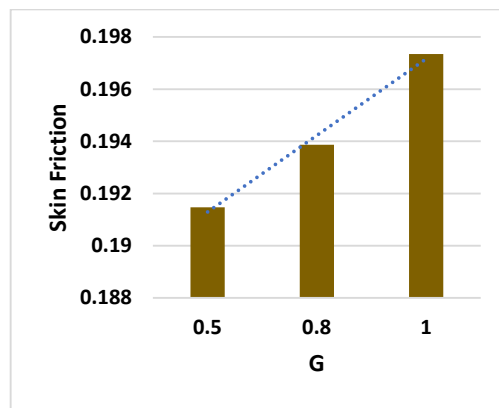
(a)
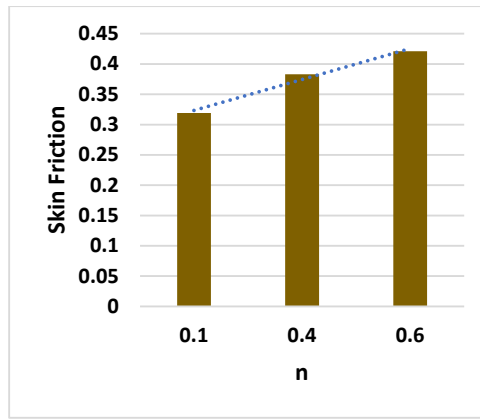
(**b**)

Figure 18. (**a**,**b**) G and n attachment with skin friction.

Figure 19 investigated the influence of θ_w and θ_r on the Nusselt number. A positive change in θ_w amplifies the nonlinear thermal radiation phenomenon which amplifies the heat transmission rate. The heat transmission rate diminishes by enhancing θ_r.

(**a**)

(**b**)
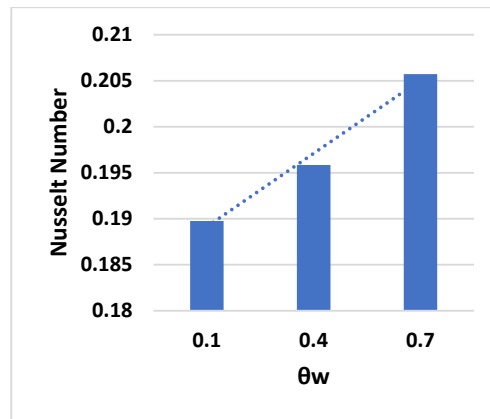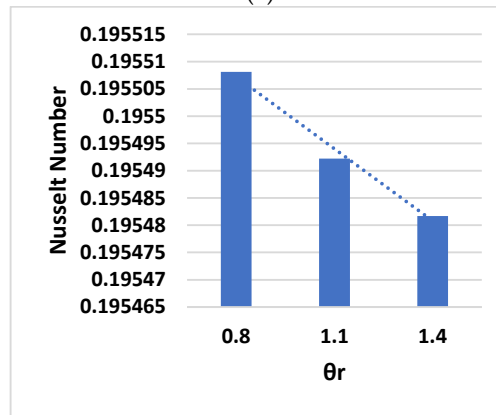
Figure 19. (**a**,**b**) θ_w and θ_r attachment with the Nusselt number.

The impact of both N_t and N_t on the heat transfer rate is displayed n Figure 20. Both N_t and N_b are important parameters of the Buongiorno nanofluid model. It is well established that the addition of nanoparticles in the base fluid amplifies the heat transmission phenomenon. That is why a variation in N_t and N_b amplifies the Nusselt number.
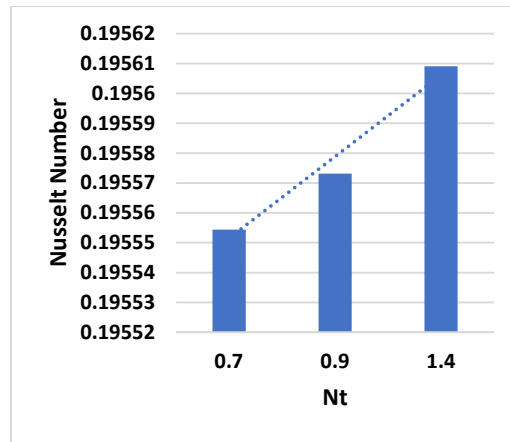
(a)
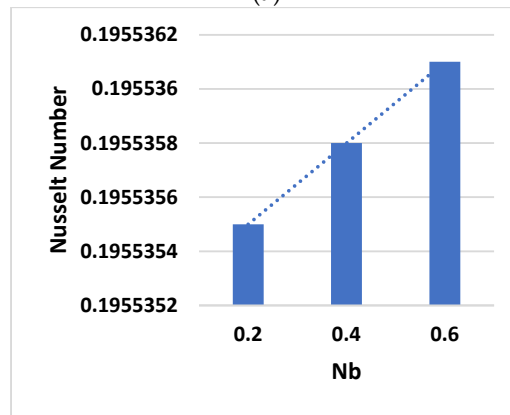
(b)

Figure 20. (**a**,**b**) N_t and N_b attachment with Nusselt number.

A positive variation in N and Pr depreciates the Nusselt number as shown in Figure 21. A continuous supply of nonlinear thermal radiation excites the conduction process among the molecules of the fluid. Molecules of the fluid collide more randomly. The Nusselt number is a ratio of heat transfer by convection to heat transfer by conductivity. The Nusselt number is inversely related to the conduction phenomenon. So, an increment in N depreciates the heat transfer Nusselt number. Thermal diffusivity lessens by augmenting Pr which diminishes the heat transfer rate.
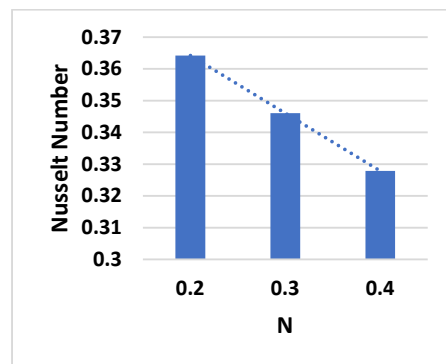
(a)
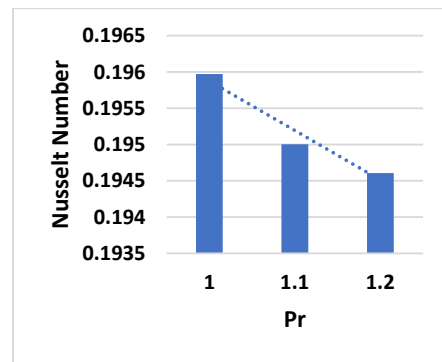
(**b**)

Figure 21. (**a**,**b**) N and Pr attachment with Nusselt number.

Figure 22 investigates the impact of thermal conductivity ε_1 and molecular diffusivity ε_2 on the Nusselt number. Diffusivity is related to concentration. A positive variation in diffusivity increases the concentration which amplifies the concentration and diminishes the liquid temperature and heat transmission rate. A variation in thermal conductivity magnifies the temperature within the liquid and depreciates the heat transfer rate phenomenon.

(**a**)

(**b**)
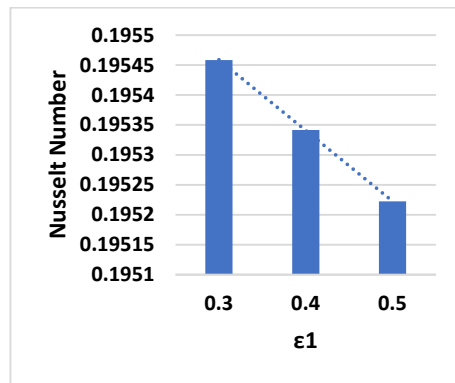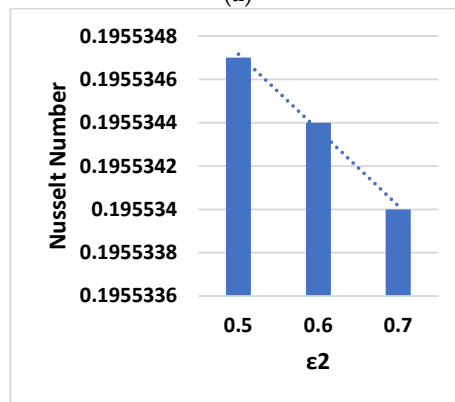
Figure 22. (**a**,**b**) ε_1 and ε_2 attachment with Nusselt number.

Table 2 is designed to reflect the impact of various dimensionless parameters that appear during the numerical simulation of the problem on the frictional force coefficient. It is remarked from the table that magnification in We, θ_r decreases the surface drag coefficient but skin friction amplifies in the case of G and N.

Table 2. Tabulation of skin friction Cross fluid.

We	θ_r	G	N	Skin Friction
1.1				**0.747311**
1.3				0.675125
1.5				0.531447
	0.1			0.511412
	0.3			0.340778
	0.5			0.293925
		0.5		0.191472
		0.8		0.193867
		1		0.197345
			0.1	0.318987
			0.4	0.383099
			0.6	0.421181

The trial case of Nusselt quantity for the status of various dimensionless parameters is highlighted in Table 3. It is noted that a positive change in θ_w, N_t, N_b and ε_1 provides magnification in the heat transmission rate. The Nusselt quantity diminishes for the case of the rest of the parameters, θ_r, N, Pr and ε_2.

Table 3. Tabulation of Nusselt number Cross fluid.

θ_w	θ_r	N_t	N_b	N	Pr	ε_1	ε_2	Nusselt Number
0.1	0.5	0.3	0.3	0.1	0.7	0.1	0.2	0.189769
0.4								0.1958574
0.7								0.1967127
	0.8							0.1955081
	1.1							0.1954922
	1.4							0.1954817
		0.7						0.1955544
		0.9						0.1955731
		1.4						0.1956091
			0.2					0.1965355
			0.4					0.1985558
			0.6					0.1995958
				0.2				0.3642232
				0.3				0.3460589
				0.4				0.3278681
					1.0			0.1959707
					1.1			0.1930041
					1.2			0.1956082
						0.3		0.1954585
						0.4		0.1955415
						0.5		0.1957222
							0.5	0.1955347
							0.6	0.1955344
							0.7	0.1955346

7. Conclusions

Two-dimensional Cross fluid past a stretchable plate under the effect of Buongiorno nanofluid has been considered. The nonlinear PDEs with the inclusion of various effects were converted into ODEs and tackled numerically with the utilization of the Lobatto IIIA scheme. Some conclusive remarks from the present study are mentioned below.

- An incremental change in variable temperature ε_1 and molecular diffusivities ε_2 diminishes the heat transfer rate.
- An amplification in unsteady parameter A improves the velocity field.
- The fluid velocity diminishes by escalating the Weissenberg number We and power-law index n.
- A positive variation in the Grashoff number G and thermal radiation N amplifies the temperature field.
- The temperature of the fluid escalates by improving N, θ_w and ε_1.
- Both N and Pr deteriorate the Nusselt number phenomenon.
- The dimensionless parameters G and n magnify the surface drag coefficient.

8. Future Directions

This work can be extended to a hybridity nanofluid model with an inclined magnetic field and heart attack diseases can be controlled by nanoparticles with a magnetic effect. The adopted method of the paper can be implemented in the research articles reported in [40–53] to quantify more physically reliable and numerically stable solutions and to present them as linear models with some criteria for the assessment of the R-Squared, standard error, and p-level.

Author Contributions: A.D., T.S., S.Z.H.S., W.J. and M.R.E.: Conceptualization, Formal analysis, Writing—original draft, Writing—review & editing. A.A., S.M.H., M.R.E., M.B.H. and M.K.: Data curation, Investigation, Methodology, Writing—original draft, Writing—review & editing. A.D., W.J., M.R.E. and M.B.H.: Software, Formal analysis, Writing—review & editing. M.R.E., S.M.H. and M.A.: Data curation, A.D., W.J. and M.R.E. Methodology, S.M.H. and M.A. funding, A.A., W.J. and M.R.E. Writing—review & editing. All authors have read and agreed to the published version of the manuscript.

Nomenclature

A	Unsteadiness parameter	U_0	Reference velocity
A_1	First Rivilin Erickson tensor	U_w	Stretching velocity
(a, b, c)	Dimensionless constants	V	Velocity profile
b	Chemotaxis constant	$v_w > 0$	Blowing
c_f	Skin friction	$v_w < 0$	Suction
c_p	Specific heat	x, y	space coordinates
C	Concentration profile	We	Weissenberg number
D	Solute diffusivity	z, r	Space variable
D_B	Diffusion coefficient of Brownian	β_T	Thermal expansion coefficient

$D(C)$	Concentration diffusivity	$\delta < 0$	Gases
D_n	Microorganisms' diffusion coefficient	$\delta > 0$	Liquids
D_T	Diffusion coefficient of thermophoresis	(δ, T_Γ)	Thermal state and thermal property
g	Gravitational acceleration	γ	Shear strain
G_c	Grashoff number (Mass)	$\dot{\gamma}$	Shear rate
G_t	Grashoff number (thermal)	ϵ_1	Variable thermal conductivity
k	Thermal conductivity	ϵ_2	Variable molecular diffusivity
k^*	Mean absorption coefficient	η	Dimensionless variable
k_∞	Infinite conductivity	$\eta_0(T)$	Dynamic viscosity
l	Characteristics length	θ_r	Variable viscosity
n	Power law index	θ_w	Temperature ratio parameter
Nu	Nusselt number	μ	Viscosity
p	Pressure	μ_0	Zero shear rate viscosity
Pr	Prandtl number	μ_∞	Infinite shear rate viscosity
q_w	Wall shear stress	ν	Kinematic viscosity
Rb	Bioconvection Rayleigh number	ρ	Fluid density
Re	Reynold number	ρ_f	Density of nanofluid
Sc	Schmidt number	ρ_p	Density of nanoparticles
$S < 0$	Injection	$(\rho c_p)_f$	Heat capacity of nanofluid
$S > 0$	Suction	$(\rho c_p)_p$	Heat capacity of nanoparticles
T	Temperature profile	σ	Electrical conductivity
T_w, C_w	Wall temperature and concentration	σ^*	Stefan-Boltzman constant
T_∞, C_∞	Ambient temperature and concentration	τ	Cauchy stress tensor
u, v	Velocity components	τ_{rx}	Heat flux
ODEs	Ordinary differential equation	ψ	Stream function
PDEs	Partial differential equation	Γ	Relaxation time constant

References

1. Sabir, Z.; Ayub, A.; Guirao, J.L.; Bhatti, S.; Shah, S.Z.H. The effects of activation energy and thermophoretic diffusion of nanoparticles on steady micropolar fluid along with Brownian motion. *Adv. Mater. Sci. Eng.* **2020**, *2020*, 2010568.
2. Ayub, A.; Wahab, H.A.; Shah, S.Z.; Shah, S.L.; Darvesh, A.; Haider, A.; Sabir, Z. Interpretation of infinite shear rate viscosity and a nonuniform heat sink/source on a 3D radiative cross nanofluid with buoyancy assisting/opposing flow. *Heat Transf.* **2021**, *50*, 4192–4232.
3. Ayub, A.; Wahab, H.A.; Sabir, Z.; Arbi, A. A note on heat transport with aspect of magnetic dipole and higher order chemical process for steady micropolar fluid. *Comput. Overv. Fluid Struct. Interact.* **2020**, *97*, 97–120.
4. Shah, S.Z.H.; Ayub, A.; Sabir, Z.; Adel, W.; Shah, N.A.; Yook, S.J. Insight into the dynamics of time-dependent cross nanofluid on a melting surface subject to cubic autocatalysis. *Case Stud. Therm. Eng.* **2021**, *27*, 101227.
5. Wahab, H.A.; Hussain Shah, S.Z.; Ayub, A.; Sabir, Z.; Bilal, M.; Altamirano, G.C. Multiple characteristics of three-dimensional radiative Cross fluid with velocity slip and inclined magnetic field over a stretching sheet. *Heat Transf.* **2021**, *50*, 3325–3341.
6. Ayub, A.; Sabir, Z.; Altamirano, G.C.; Sadat, R.; Ali, M.R. Characteristics of melting heat transport of blood with time-dependent cross-nanofluid model using Keller–Box and BVP4C method. *Eng. Comput.* **2021**, *38*, 3705–3719.
7. Ayub, A.; Sabir, Z.; Le, D.N.; Aly, A.A. Nanoscale heat and mass transport of magnetized 3-D chemically radiative hybrid nanofluid with orthogonal/inclined magnetic field along rotating sheet. *Case Stud. Therm. Eng.* **2021**, *26*, 101193.
8. Ayub, A.; Wahab, H.A.; Balubaid, M.; Mahmoud, S.R.; Ali, M.R.; Sadat, R. Analysis of the nanoscale heat transport and Lorentz force based on the time-dependent Cross nanofluid. *Eng. Comput.* 2022, *in press*.
9. Shah, S.Z.; Wahab, H.A.; Ayub, A.; Sabir, Z.; haider, A.; Shah, S.L. Higher order chemical process with heat transport of magnetized cross nanofluid over wedge geometry. *Heat Transf.* **2021**, *50*, 3196–3219.
10. Ayub, A.; Darvesh, A.; Altamirano, G.C.; Sabir, Z. Nanoscale energy transport of inclined magnetized 3D hybrid nanofluid with Lobatto IIIA scheme. *Heat Transf.* **2021**, *50*, 6465–6490.
11. Ayub, A.; Wahab, H.A.; Hussain Shah, S.Z.; Shah, S.L.; Sabir, Z.; Bhatti, S. On heated surface transport of heat bearing thermal radiation and MHD Cross flow with effects of nonuniform heat sink/source and buoyancy opposing/assisting flow. *Heat Transf.* **2021**, *50*, 6110–6128.
12. Ayub, A.; Sabir, Z.; Shah, S.Z.H.; Wahab, H.A.; Sadat, R.; Ali, M.R. Effects of homogeneous-heterogeneous and Lorentz forces on 3-D radiative magnetized cross nanofluid using two rotating disks. *Int. Commun. Heat Mass Transf.* **2022**, *130*, 105778.

13. Ayub, A.; Sabir, Z.; Shah, S.Z.H.; Mahmoud, S.R.; Algarni, A.; Sadat, R.; Ali, M.R. Aspects of infinite shear rate viscosity and heat transport of magnetized Carreau nanofluid. *Eur. Phys. J. Plus* **2022**, *137*, 247.

14. Ayub, A.; Shah, S.Z.H.; Sabir, Z.; Rao, N.S.; Sadat, R.; Ali, M.R. Spectral relaxation approach and velocity slip stagnation point flow of inclined magnetized cross-nanofluid with a quadratic multiple regression model. *Waves Random Complex Media* 2022, *in press*.

15. Bilal, M.; Khan, S.; Ali, F.; Arif, M.; Khan, I.; Nisar, K.S. Couette flow of viscoelastic dusty fluid in a rotating frame along with the heat transfer. *Sci. Rep.* **2021**, *11*, 506.

16. Azam, M.; Xu, T.; Khan, M. Numerical simulation for variable thermal properties and heat source/sink in flow of Cross nanofluid over a moving cylinder. *Int. Commun. Heat Mass Transf.* **2020**, *118*, 104832.

17. Azam, M.; Xu, T.; Shakoor, A.; Khan, M. Effects of Arrhenius activation energy in development of covalent bonding in axisymmetric flow of radiative-Cross nanofluid. *Int. Commun. Heat Mass Transf.* **2020**, *113*, 104547.

18. Alshomrani, A.S.; Ullah, M.Z.; Baleanu, D. Importance of multiple slips on bioconvection flow of cross nanofluid past a wedge with gyrotactic motile microorganisms. *Case Stud. Therm. Eng.* **2020**, *22*, 100798.

19. Haq, F.; Saleem, M.; ur Rahman, M. Investigation of natural bio-convective flow of Cross nanofluid containing gyrotactic microorganisms subject to activation energy and magnetic field. *Phys. Scr.* **2020**, *95*, 105219.

20. Shi, Q.H.; Hamid, A.; Khan, M.I.; Kumar, R.N.; Gowda, R.J.; Prasannakumara, B.C.; Shah, N.A.; Khan, S.U.; Chung, J.D. Numerical study of bio-convection flow of magneto-cross nanofluid containing gyrotactic microorganisms with activation energy. *Sci. Rep.* **2021**, *11*, 16030.

21. Xiong, P.Y.; Hamid, A.; Chu, Y.M.; Khan, M.I.; Gowda, R.J.; Kumar, R.N.; Prasannakumara, B.C.; Qayyum, S. Dynamics of multiple solutions of Darcy–Forchheimer saturated flow of Cross nanofluid by a vertical thin needle point. *Eur. Phys. J. Plus* **2021**, *136*, 315.

22. Waqas, H.; Khan, S.A.; Khan, S.U.; Khan, M.I.; Kadry, S.; Chu, Y.M. Falkner-Skan time-dependent bioconvrction flow of cross nanofluid with nonlinear thermal radiation, activation energy and melting process. *Int. Commun. Heat Mass Transf.* **2021**, *120*, 105028.

23. Choi, S.U.; Eastman, J.A. *Enhancing Thermal Conductivity of Fluids with Nanoparticles*; No. ANL/MSD/CP-84938; CONF-951135-29; Argonne National Lab. (ANL): Argonne, IL, USA, 1995.

24. Said, Z.; Hachicha, A.A.; Aberoumand, S.; Yousef, B.A.; Sayed, E.T.; Bellos, E. Recent advances on nanofluids for low to medium temperature solar collectors: Energy, exergy, economic analysis and environmental impact. *Prog. Energy Combust. Sci.* **2021**, *84*, 100898.

25. Sheikholeslami, M.; Farshad, S.A.; Ebrahimpour, Z.; Said, Z. Recent progress on flat plate solar collectors and photovoltaic systems in the presence of nanofluid: A review. *J. Clean. Prod.* **2021**, *293*, 126119.

26. Marzougui, S.; Mebarek-Oudina, F.; Assia, A.; Magherbi, M.; Shah, Z.; Ramesh, K. Entropy generation on magneto-convective flow of copper–water nanofluid in a cavity with chamfers. *J. Therm. Anal. Calorim.* **2021**, *143*, 2203–2214.

27. Muhammad, T.; Waqas, H.; Khan, S.A.; Ellahi, R.; Sait, S.M. Significance of nonlinear thermal radiation in 3D Eyring–Powell nanofluid flow with Arrhenius activation energy. *J. Therm. Anal. Calorim.* **2021**, *143*, 929–944.

28. Said, Z.; Sundar, L.S.; Tiwari, A.K.; Ali, H.M.; Sheikholeslami, M.; Bellos, E.; Babar, H. Recent advances on the fundamental physical phenomena behind stability, dynamic motion, thermophysical properties, heat transport, applications, and challenges of nanofluids. *Phys. Rep.* **2021**, *946*, 1–94.

29. Meibodi, S.S.; Kianifar, A.; Mahian, O.; Wongwises, S. Second law analysis of a nanofluid-based solar collector using experimental data. *J. Therm. Anal. Calorim.* **2016**, *126*, 617–625.

30. Jalil, M.; Asghar, S.; Yasmeen, S. An exact solution of MHD boundary layer flow of dusty fluid over a stretching surface. *Math. Probl. Eng.* **2017**, *2017*, 2307469.

31. Raju, C.S.K.; Sandeep, N.; Sulochana, C.; Sugunamma, V.; Babu, M.J. Radiation, inclined magnetic field and cross-diffusion effects on flow over a stretching surface. *J. Niger. Math. Soc.* **2015**, *34*, 169–180.

32. Akinbobola, T.E.; Okoya, S.S. The flow of second grade fluid over a stretching sheet with variable thermal conductivity and viscosity in the presence of heat source/sink. *J. Niger. Math. Soc.* **2015**, *34*, 331–342.

33. Ahmad, N.; Siddiqui, Z.; Mishra, M. Boundary layer flow and heat transfer past a stretching plate with variable thermal conductivity. *Int. J. Non-Linear Mech.* **2010**, *45*, 306–309.

34. Okoya, S.S.; Hassan, A.R.; Salawu, S.O. On free convection flow of a moving vertical permeable plate with quadratic Boussinesq approximation and variable thermal conductivity. *Heat Transf. Res.* **2021**, *52*, 55–66.

35. Shoaib, M.; Raja, M.A.Z.; Sabir, T.; Awais, M.; Islam, S.; Shah, Z.; Kumam, P. Numerical analysis of 3-D MHD hybrid nanofluid over a rotational disk in presence of thermal radiation with Joule heating and viscous dissipation effects using Lobatto IIIA technique. *Alex. Eng. J.* **2021**, *60*, 3605–3619.

36. Ahmad, I.; Cheema, T.N.; Raja, M.A.Z.; Awan, S.E.; Alias, S.B.; Iqbal, S.; Shoaib, M. A novel application of Lobatto IIIA solver for numerical treatment of mixed convection nanofluidic model. *Sci. Rep.* **2021**, *11*, 4452.

37. Hayat, T.; Asad, S.; Mustafa, M.; Alsaedi, A. Radiation effects on the flow of Powell-Eyring fluid past an unsteady inclined stretching sheet with non-uniform heat source/sink. *PLoS ONE* **2014**, *9*, e103214.

38. Waqas, H.; Rafique, S.; Khalid, S.; Ahmad, F.; Hussain, S. Thermal radiation effects on unsteady MHD flow of Casson fluids through porous medium over a permeable shrinking sheet. *J. Appl. Environ. Biol. Sci.* **2017**, *7*, 201–209.

39. Raghunath, K.; Gulle, N.; Vaddemani, R.R.; Mopuri, O. Unsteady MHD fluid flow past an inclined vertical porous plate in the presence of chemical reaction with aligned magnetic field, radiation, and Soret effects. *Heat Transf.* **2022**, *51*, 2742–2760.

40. Hussain, S.M.; Jamshed, W.; Safdar, R.; Shahzad, F.; Mohd Nasir, N.A.A.; Ullah, I. Chemical reaction and thermal characteris-tiecs of Maxwell nanofluid flow-through solar collector as a potential solar energy cooling application: A modified Buongiorno's model. *Energy Environ.* 2022, *in press.*

41. Hussain, S.M. Irreversibility Analysis of Time Dependent Magnetically Driven Flow of Sutterby Hybrid Nanofluid: A Thermal Mathematical Model. *Waves Random Complex Media* **2022**. https://doi.org/10.1080/17455030.2022.2089369.

42. Hussain, S.M. Thermal Enhanced Hybrid of Copper-Zirconium Dioxide/Ethylene Glycol nanofluid Flowing in Solar Collector of Water-Pump Application. *Waves Random Complex Media* **2022**. https://doi.org/10.1080/17455030.2022.2066734.

43. Sajid, T.; Jamshed, W.; Safdar, R.; Hussain, S.M.; Shahzad, F.; Bilal, M.; Rehman, Z.; Rahman, M.M.; Pasha, A.A. Features and aspects of radioactive flow and slippage velocity on rotating two-phase Prandtl nanofluid with zero mass fluxing and convective constraints. *Int. Commun. Heat Mass Transf.* **2022**, *136*, 106180.

44. Hussain, S.M.; Jamshed, W.; Eid, M.R. Solar-HVAC Thermal Investigation Utilizing (Cu-AA7075/C6H9NaO7) MHD-Driven Hybrid Nanofluid Rotating Flow via Second-Order Convergent Technique: A Novel Engineering Study. *Arab. J. Sci. Eng.* **2022**. https://doi.org/10.1007/s13369-022-07140-6.

45. Shahzad, F.; Jamshed, W.; Pasha, A.A.; Safdar, R.; Alam, M.M.; Arshad, M.; Hussain, S.M.; Krawczuk, M. Thermal Cooling Process by Nanofluid Flowing near Stagnating Point of Expanding Surface under Induced Magnetism Force: A Computational Case Study. *Case Stud. Therm. Eng.* **2022**, *36*, 102190.

46. Hussain, S.M.; Mishra, M.R.; Seth, G.S.; Chamkha, A.J. Dynamics of heat absorbing and radiative hydromagnetic nanofluids through a stretching surface with chemical reaction and viscous dissipation. *Part-E J. Proc. Mech. Eng.* **2022**. https://doi.org/10.1177/09544089221096103.

47. Hussain, S.M.; Sharma, R.; Chamkha, A.J. Numerical and statistical exploration on the dynamics of water conveying Cu-Al2O3 hybrid nanofluid flow over an exponentially stretchable sheet with Navier's partial slip and thermal jump conditions. *Chin. J. Phys.* **2022**, *75*, 120–138.

48. Jamshed, W.; Devi, S.U.S.; Prakash MHussain, S.M.; Eid, M.R.; Nisar, K.S.; Muhammad, T. Entropy Amplified Solitary Phase Relative Probe on Engine Oil Based Hybrid Nanofluid. *Chin. J. Phys.* **2022**, *77*, 1654–1681.

49. Hussain, S.M.; Jamshed, W.; Pasha, A.A.; Adil, M.; Akram, M. Galerkin finite element solution for electromagnetic radiative impact on viscid Williamson two-phase nanofluid flow via extendable surface. *Int. Commun. Heat Mass Transf.* **2022**, *137*, 106243.

50. Hussain, S.M.; Goud, B.S.; Madheshwaran, P.; Jamshed, W.; Pasha, A.A.; Safdar, R.; Arshad, M.; Ibrahim, R.W.; Ahmad, M.K. Effectiveness of Nonuniform Heat Generation (Sink) and Thermal Characterization of a Carreau Fluid Flowing across a Non-linear Elongating Cylinder: A Numerical Study. *ACS Omega* **2022**, *7*, 25309–25320.

51. Parvin, S.; Isa, S.S.P.M.; Al-Duais, F.S.; Hussain, S.M.; Jamshed, W.; Safdar, R.; Eid, M.R. The flow, thermal and mass properties of Soret-Dufour model of magnetized Maxwell nanofluid flow over a shrinkage inclined surface. *PLoS ONE* **2022**, *17*, e0267148.

52. Jamshed, W.; Eid, M.R.; Hussain, S.M.; Abderrahmane, A.; Safdar, R.; Younis, O.; Pasha, A.A. Physical Specifications of MHD Mixed Convective of Ostwald–de Waele Nanofluids in a Vented-Cavity with Inner Elliptic Cylinder. *Int. Commun. Heat Mass Transf.* **2022**, *134*, 106038.

53. Shahzad, F.; Jamshed, W.; Safdar, R.; Hussain, S.M.; Nasir, M.N.A.A.; Dhange, M.; Nisar, K.S.; Eid, M.R.; Sohail, M.; Alsehli, M.; et al. Thermal Analysis Characterization of Solar Powered Ship Using Oldroyd Hybrid Nanofluids in Parabolic Trough Solar Collector: An Optimal Thermal Application. *Nanotech. Rev.* **2022**, *11*, 2015–2037.